Journal of Multidisciplinary Engineering Science and Technology (JMEST)
ISSN: 2458-9403
Vol. 12 Issue 7, July - 2025

Direct-Phase Variable Performance of a Distributed Winding Synchronous Reluctance Generator with Permanent Magnet

Obuah Emmanuel Chinweikpe
Department of Electrical and Electronic Engineering
Rivers State University
Port Harcourt, Nigeria
emmanuel.obuah@ust.edu.ng

Biragbara Peace
Department of Electrical and Electronic Engineering
Rivers State University
Port Harcourt, Nigeria

Eze Uche Chimka
Department of Electrical and Electronic Engineering
Rivers State University
Port Harcourt, Nigeria

Ubong Jeremiah Joseph
Department of Electrical and Electronic Engineering
Rivers State University
Port Harcourt, Nigeria

Abstract*— *Dynamic performance of a three-phase synchronous reluctance generator with permanent magnet (PM) based on Winding Function Theory (WFT) is presented here in natural frame for a generator with distributed winding (DW stator). Based on WFT, the equations for the turn function, winding function and inductance of the generator were obtained considering the space harmonics. The calculated inductance model was the used to predict the dynamic behavior of the under various operating conditions. Such as no load and load and loss of load probability. Self-excitation is achieved via balanced three-phase capacitors connected across the stator windings as well as the permanent magnet flux. It is realized that the generator can simultaneously supply good voltage through its terminals, in both normal and transient conditions within its rating without any transients in its output variables. However, slight transient behavior is noticed in the output variables when the generator loses load. Verification of the generator equations was done in MATLAB/Simulink tool.

Keywords*— *Direct-Phase Variable, Dynamic performance, load disturbance, MATLAB/Simulink, permanent magnet, synchronous reluctance generator.

I. INTRODUCTION

The need for electrical energy globally cannot be over emphasized. Electrical energy promotes economic activities of countries, contributes, and facilitate learnings and have huge impact in governance.

Different electric generators that can generate electricity exist. These generators include field excited machines and self-excited machines. Field excited generators are mainly used for centralized electricity generation, despite their high maintenance cost. In areas where the grid is not present, or situations where the grid supply cannot meet the demand, renewable energy technologies such as solar, geothermal and wind turbine are viable options for alternative energy technologies [1]. The self-excited generators are mainly employed for renewable energy technologies like wind energy conversion systems [2] and [3].

The synchronous reluctance generators belong to the family of self-excited generators like the self-excited induction generator and permanent magnet synchronous generators. The key consideration for the use of self-excited induction generator for this purpose include cost and simplicity of construction. The self-excited induction generator is also rugged in construction and protected against excessive overload and short circuit fault. The generator also requires no external direct current supply for excitation and has better transient performance due to its damping winding features.

A major drawback of this generator is the fact that it suffers from poor voltage and frequency regulation with changes in load and prime mover speed, hence requires voltage and frequency stabilizing circuit [4]. Due to this inherent bottleneck which calls for stabilizing circuit, the cost of installation of self-excited induction generator increases [5]. To overcome the problem of unstable voltage and frequency with varying load in self-excited induction generator, researchers shifted attention to synchronous reluctance machines, devoted mainly development and improvement of the rotor of the induction machine [6], [7]. Hence, the synchronous generator, possesses the characteristic of induction machine and synchronous machine. The working principle or operational steps of the self-excitation operation of reluctance generators is a well-known phenomenon, which include the use of existing remnant flux and magnetic saturation like that of induction

generators [8], [9]. But most studies of the three-phase self-excited reluctance generators use d-q reference frame techniques, which have been extensively researched [10], [4], and [11].

The chief benefit of the synchronous reluctance machine is that the output voltage and frequency is constant, which is because of the leading current produced by the excitation capacitor [3]; however, its output power is very small compared to the permanent magnet machine. This means that the size of the machine could be invariably large compared to the induction machine of the same rating by way of design.

The first time a study in direct phase-variable model simulation of synchronous machines was reported in when Staton, Miller and Wood, work on saliency of the machine as a way of predicting machine performance during faults and unbalanced loading conditions [12]. Further work was done on the machine when the effect of saturation was introduced [13]. One general feature of the studies of [12] and [13] is that all neglected higher order harmonics. A study found in literature for synchronous reluctance generator in natural variable for a single-phase reluctance generator was also done by [14]. The study first, employed the winding function approach to calculate the inductance of the machine before furthering its finding on event of short circuit condition.

According to [10], the rotor of synchronous reluctance generator can be configured to make provision for insertion of permanent magnet. This has been demonstrated for a gased rotor type in d-q referencing frame [3]. A notable work that simulated permanent magnet machine in natural variable model was done by Aliyu [15] for motor, and Arkadan and Demerdash [16] for three-phase generator. Since the study by [16], it is not clear in the literature whether any work has been carried out recently considering performance of the generator in natural variable frame considering loss-of-load of probability. This study shall consider the dynamic performance analysis of a self-excited three-phase cageless rotor reluctance generator with permanent magnet using the actual machine geometry for calculation of inductance and analysis of the machine instead of the use of traditional winding function, which uses Fourier model. In traditional winding function procedures where Fourier expression is employed, only the fundamental components of winding functions and only the average plus the second harmonic component of the inverse airgap functions are used. For accuracy, the effects of stator slots are included in a way all the harmonics are considered. A computer simulation of the developed model of the generator is done in the MATLAB/Simulink environment [17] and closely studied for different loading conditions. The results of these simulations are then analyzed.

II. MATERIALS AND METHOD

A. Machine Analysis based on Winding Function

The machine clock diagram is presented in Fig. 1 for a double layer full pitched 36 slots 4 poles distributed winding (DW) machine. A+ is the coil carrying current outward the paper from phase A. A- is the coil carrying current inward of the paper from phase A. B+ is the coil carrying current outward into the paper from phase B. B- is the coil carrying current inward of the paper from phase B. C+ is the coil carrying current outward the paper from phase C. C- is the coil carrying current inward of the paper from phase C. The machine coil arrangement has 12 coils placed in each of the three-phase. Under each pole region, the number of coils for each phase is 3. The angle between adjacent slots is 20^o, and the angle between two sides of the same coil is 180^o.

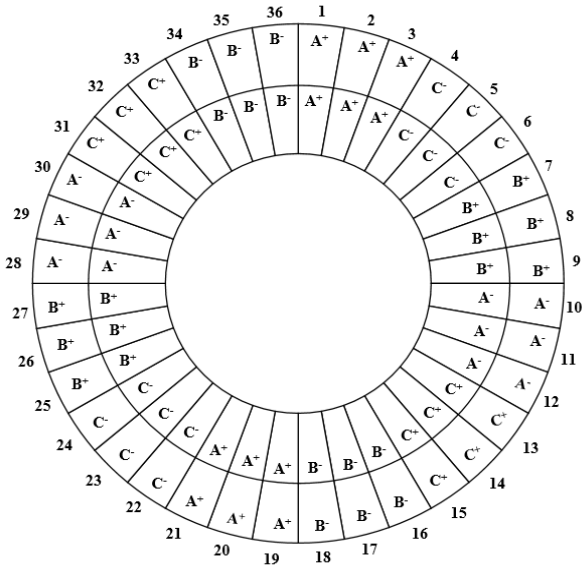

Fig 1. Clock diagram of the full pitched double layer distribution winding machine

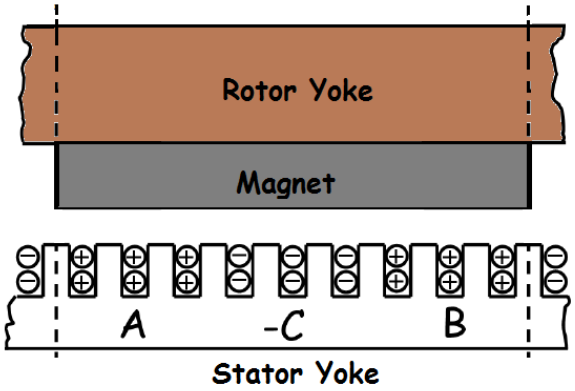

Fig 2. Coil winding partner for the double layer 4 pole, 36 slots machine

Now, consider the winding arrangement for the 4-poleslots machine in Fig2. The derived equations that described the actual turns and winding function of the machine for phase A is expressed as (1) and (2) respectively, using the machine geometry. The equations for phase B and C are

similar when the stator angle is shifted accordingly by 2π/3. The Fourier expression is given in (3)

$$n_A(\theta_s)=\begin{Bmatrix} N_C & 5\pi/18>\theta_S\le\pi/9 \\ 2N_C & \text{for } \pi/9>\theta_S\le\pi/6 \\ 3N_C & \pi/6>\theta_S\le 10\pi/18 \\ 0 & others \end{Bmatrix} \quad (1)$$

$$N_A(\theta_s)=\begin{Bmatrix} N_C/2 & 5\pi/18>\theta_S\le\pi/9 \\ 2N_C/2 & \text{for } \pi/9>\theta_S\le\pi/6 \\ 3N_C/2 & \pi/6>\theta_S\le 10\pi/18 \\ 0 & others \end{Bmatrix} \quad (2)$$

$$N_X(\theta_s)=\frac{4N_cK_w}{\pi P}\cos\left(P\theta_s-r\frac{2\pi}{m}\right) \quad (3)$$

where $r=0,1,2$ for the phase $A, B,$ C respectively. K_w is the fundamental winding factor, N_c is the number of turns of machine winding per phase, m is the number of phase.

The MMF plot of the turn and winding functions are illustrated in Fig. 3 and 4 respectively. The plot describes the position of the machine windings in the stator from equations (1) and (2) respectively. The machine coil windings in the stator slot are well distributed, which implies the machine MMF in each phase have the same or regular pattern or shape. It is seen that the winding functions corresponding to the stator windings are defined as a function of stator angle according to their winding layouts in Fig 1. Fourier model expressed in equation (3) is used to obtain the sinusoidal part of the machine MMF.

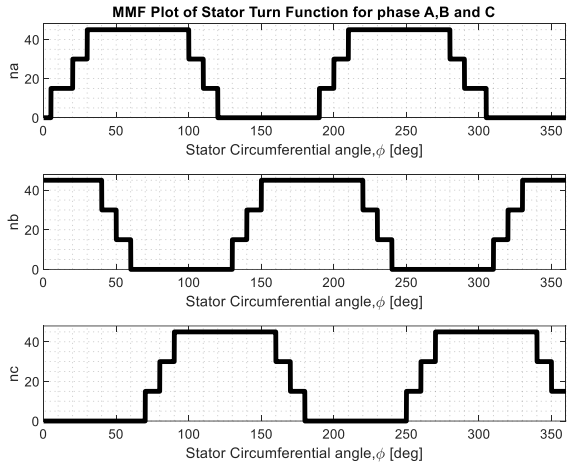

Fig.3 Turn function of the studied machine for the three phase

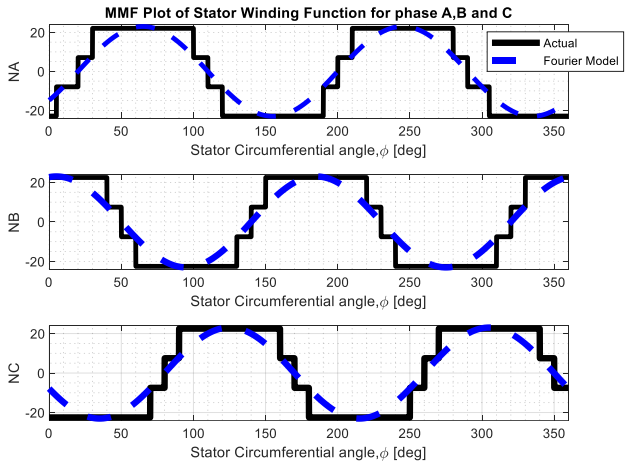

Fig.4. Winding function of the studied machine (Actual and Fourier)

The space harmonics order of the machine for phase A due to the winding arrangement is shown in Fig 5 using Fast Fourier Transform (FFT). The Fourier analysis showed that the air gap MMF produced by the machine. The two most significant space-harmonics are the fundamental 1st and the 5th. The other harmonics are minimized. The is beneficial in terms of better machine utilization. The fundamental space-harmonic amplitude is 27.3. The fundamental MMF wave amplitude and higher space-harmonic of order v is gotten from the expression in equation (3). During normal operation, the machine starts with the first harmonic rotating in synchronism with the rotor magnetic field to produce electromagnetic torque. Since other harmonics are not significant, eddy current loss is also minimized.

$$MMF_{A(1)}=\frac{4}{\pi}\frac{N_C}{v2}I\sqrt{2} \quad (4)$$

where N_C is the number of turns of coil, I is the alternating current rms value, v is harmonic order number.

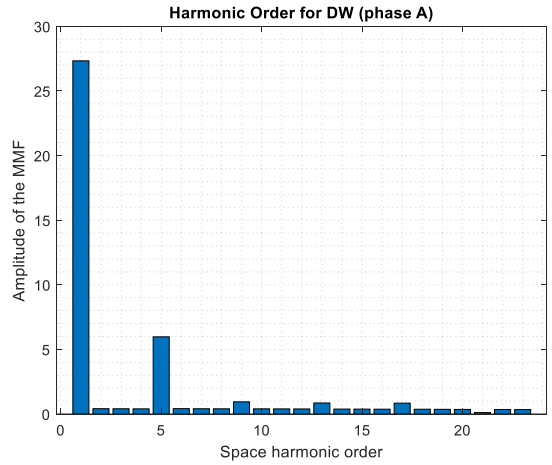

Fig.5. Harmonic order of the studied machine for phase A

According to Winding Function Method for an AC machine, the self-inductance of phase *X* can be calculated as:

$$L_X = \frac{\mu_o l_s r_s}{g_{eff}(\theta_s)} \int_0^{2\pi} N_Y(\theta_s) d\theta_s \quad (5)$$

The term g_{eff} is the effective air-gap length, N_Y is the turns function, μ_o is the permeability of free space, l_s is the stator stack length, r_s is the effective radius of the stator bore. The effective air-gap length can be given as (6).

$$g_{eff} = k_C g \quad (6)$$

K_C is the Carter air-gap Correction factor which was introduced in 1920s by F.W. Carter to provide solution to the problem of slot effect.

The expression for inverse airgap with Carter's modification, considering only the first-time varying harmonic is expressed as (7).

$$g^{-1}(\phi_s, \theta_r) = \frac{1}{2}\left(\frac{1}{g_1} + \frac{1}{g_2}\right) - \frac{\pi}{2}\left(\frac{1}{g_1} - \frac{1}{g_2}\right) \sin \pi\beta \cos 2(\phi_s - \theta_r) \quad (7)$$

where

g_1 is the air gap at pole face, g_2 is the air gap at depth between poles, β is the ratio of pole arc to pole pitch. Fig.6 illustrates the position of g_1 and g_2 is the rotor air gap.

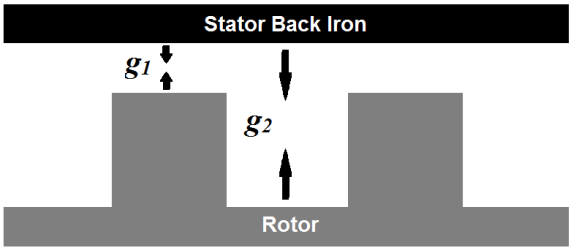

Fig. 6 A machine air gap structure to illustrate the air gap at pole and depth

Equation (5) shows that the winding expression of any stator winding does not change with rotor position, but only with stator circumferential angle Θ_s and can be easily calculated from the turn function N_Y by subtracting the average of the turn function from itself [14]. This winding function equation for calculation of the machine inductances are used to develop a MATLAB program for simulation. The plot is presented as shown in Fig. 7 for phase A of the machine only. The machine also has waveform close to the traditional sinusoidal form.

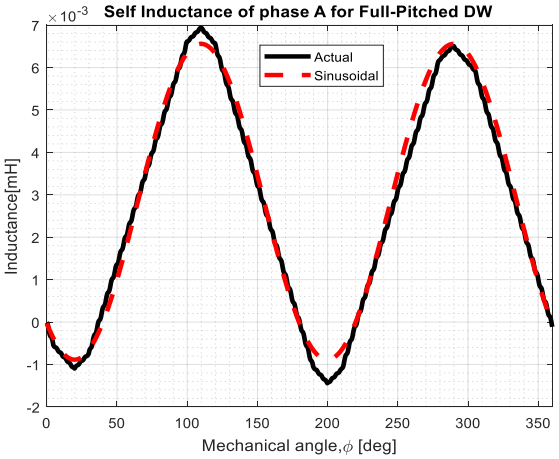

Fig. 7 Self- inductance of the studied machine for phase A

B. Dynamic Analysis of the Machne based on Direct-Phase Variable Model

To present the models that described the dynamic behaviour of the machine in natural, the machine inductance model is needed. Consider the the machine geometryin Fig 8. The modeling wil begin with the most fundamental component of the permrnent magnet machine. The magnets are assumed to be a single phase, rather than as multiple phases. The inductances will be calculated for the case in which the two coils, *A* and *B*, are treated as distinct coils, and ones which are connected in series [15].

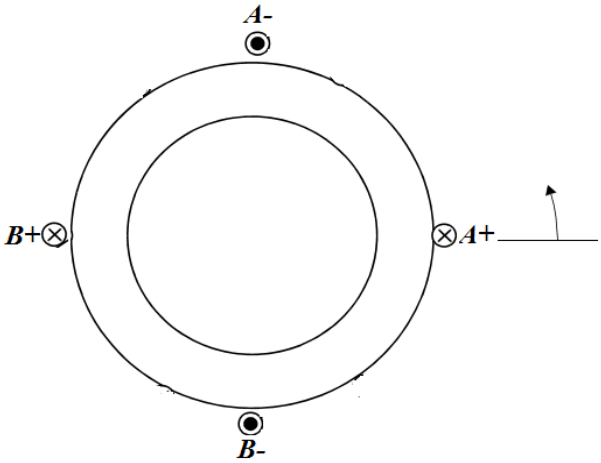

Fig. 8: A basic full pitch machine

The turn function can be expressed as (8) for the stator circumference angle, Θ_s from 0 to 2π, with *N* as number of turns.

$$\langle n(\theta_s)\rangle = \left[\frac{1}{2\pi}\int_0^{\pi} n(\theta_s)\right] = \frac{N}{4} \quad (8)$$

The self inductance of A is calculated as (9)

$$L_A = \frac{\mu_o r_s l_s}{g_{eff}}\int_0^{2\pi} N_A{}^2(\theta_s)d\theta_s = \frac{\mu_o r_s l_s}{g_{eff}}\left[\int_0^{\pi/2}\left(\frac{3N^2}{4}\right)d\theta_s + \int_{\pi}^{2\pi}\left(\frac{-N^2}{4}\right)d\theta_s\right] \quad (9)$$

Analyzing the inductance expression in (9) with effective airgap elements gives the final equation for A in equation (10).

$$L_A = \left[\frac{3}{8}\right]\frac{\pi N^2 \mu_o r_s l_s}{g_{eff}}\alpha_1 \quad (10)$$

Similarly, the inductance for between for B is calculated as (11).

$$L_B = \frac{\mu_o r_s l_s}{g_{eff}}\int_0^{2\pi} N_B(\theta_s)d\theta_s = \frac{\mu_o r_s l_s}{g_{eff}}\left[\int_{\pi}^{\frac{3\pi}{2}}\left(\frac{-N^2}{4}\right)d\theta_s\right] \quad (11)$$

Also, analyzing the inductance expression in (11) with effective airgap elements gives the final equation for B in equation (12).

$$L_B = \left[\frac{1}{8}\right] - \frac{N_c{}^2 \pi \mu_o r_s l_s}{g_{eff}}\alpha_2 \quad (12)$$

where

α_1 and α_2 are elements of effective air gap given as:

$$\alpha_1 = \alpha_2 = \frac{a}{b} \quad (13)$$

$$a = \left[\frac{g_1}{g_2} * 100\right] + g_1 \quad (14)$$

$$b = \left[\frac{g_1}{g_2} * 100\right] / g_1 \quad (15)$$

The self-inductance of each stator phase winding A and B will reach a maximum value whenever the rotor d-axis aligns with the axis of the phase winding because the reluctance of the linkage flux path is minimum. This minimum reluctance condition occurs twice during each rotation of the rotor so that the stator self-inductances are represented by a constant component and a single periodic component, the higher harmonics neglected. L_A is the constant component of the magnetizing inductance of the stator winding, L_B is the amplitudes of the second harmonics of the magnetizing inductance.

To achieve a sinusoidal field, each of the stator windings is shifted in space relative to the others by 2π/3. The self-inductances of the stator for phase B and C are given in (17) to (19).

$$L_{aa} = L_{ls} + L_A + L_B\cos[2(\theta_s)] \quad (17)$$

$$L_{bb} = L_{ls} + L_A + L_B\cos\left[\left(2\theta_s - \frac{2\pi}{3}\right)\right] \quad (18)$$

$$L_{cc} = L_{ls} + L_A + L_B\cos\left[\left(2\theta_s - \frac{4\pi}{3}\right)\right] \quad (19)$$

where L_{ls} is the stator leakage inductance.

The mutual inductance between each of the stator windings can be written as (20) to (26).

$$L_{ab} = -\frac{L_A}{2} + L_B\cos\left[\left(2\theta_2 - \frac{2\pi}{3}\right)\right] \quad (20)$$

$$L_{ba} = -\frac{L_A}{2} + L_B\cos\left[2\left(\theta_s - \frac{4\pi}{3}\right)\right] \quad (21)$$

$$L_{bc} = -\frac{L_A}{2} + L_B\cos\left[\left(2\theta_s - \frac{2\pi}{3}\right)\right] \quad (22)$$

$$L_{cb} = -\frac{L_A}{2} + L_B\cos\left[\left(2\theta_s - \frac{4\pi}{3}\right)\right] \quad (23)$$

$$L_{ca} = -\frac{L_A}{2} + L_B\cos\left[\left(2\theta_s - \frac{2\pi}{3}\right)\right] \quad (24)$$

$$L_{ac} = -\frac{L_A}{2} + L_B\cos\left[\left(2\theta_s - \frac{4\pi}{3}\right)\right] \quad (26)$$

The stator inductance can be given in matrix form in equation (27) for phase A, B and C

$$L_S = \begin{bmatrix} L_{aa} & L_{ab} & L_{ac} \\ L_{ba} & L_{bb} & L_{bc} \\ L_{ca} & L_{cb} & L_{cc} \end{bmatrix} \quad (27)$$

This inductance is related to the voltage equation of the machine given in equation (28), which is later presented in (29) for the purpose of simulation.

$$E = I_S R_S + \frac{d}{dt}\left(L_S I_S\right) + V_c \quad (28)$$

$$\frac{dI_S}{dt} = \left[E - I_S\left(R_S + \omega_r * \frac{dL_S(\theta_r)}{d\theta_r} \right) \right] * L_S(\theta_r)^{-1} - V_c \quad (29)$$

V_{ac} is the per phase capacitor voltage, which is generated using equation (30).

$$V_{ca} = \frac{1}{C}\int I_s dt \quad (30)$$

where C is the capacitance of the capacitor.

$\omega_r = \frac{d\theta_r}{dt}$, which is the rotor speed.

I_S is the stator three phase current given as:

$$I_S = \left[I_a ; \quad I_b ; \quad I_c \right] \quad (31)$$

R_S is the stator three-phase resistance, given in matrix form as (32).

$$R_S = \begin{bmatrix} R_a & 0 & 0 \\ 0 & R_b & 0 \\ 0 & 0 & R_c \end{bmatrix} \quad (32)$$

E is permanent magnet three-phase emf produced, given as

$$E = \left[E_a ; \quad E_b ; \quad E_c \right] \quad (33)$$

where

$$E_a = \lambda m \cos wt \quad (34)$$

$$E_b = \lambda m \cos\left(wt - \frac{2\pi}{3} \right) \quad (35)$$

$$E_c = \lambda m \cos\left(wt - \frac{4\pi}{3} \right) \quad (36)$$

λ_m is the permanent magnet constant flux.

The electromagnetic torque is derived in (37) using co-energy method.

$$T_e = \frac{1}{2}\left[I_S \right]^2 \frac{d\left| L_S(\theta_r) \right|}{d\theta_r} + \lambda_m \quad (37)$$

And the power output is:

$$P_o = 3V_{ac} * I_s * pf \quad (38)$$

The inductive load equation per phase is given as (39).

pf is the machine power factor.

$$L_{aL} = \frac{R_{aL}}{\omega_r}\sqrt{\left(\frac{1}{pf} \right)^2 - 1} \quad (39)$$

where

R_{aL} is the per phase resistive load. The load current is found as a state variable in (40).

$$\frac{d}{dt} I_{aL} = \frac{\left(V_{ac} - R_{aL} * I_{aL} \right)}{L_{aL}} \quad (40)$$

The active power and reactive power equation are expressed in (41) and (42) respectively.

$$P_A = 3V_{ac} * I_{aL} * pf \quad (41)$$

$$Q_R = 3V_{ac} * I_{aL} * \left(- pf \right) \quad (42)$$

III. RESULTS AND DISCUSSION

The simulation results presented in this section were obtained using MATLAB/Simulink to observe the performance of the system under the following conditions including no-load, variable loading and. Inductive and resistive load of 400 Ω, 30 mH was used. The generator relates to a balance star-connected bank capacitor, and the value of the capacitor is 80 µF per phase. A constant permanent magnet flux of 0.8 was used at 0.8 power factor. The analysis was done with unsaturated value of inductance. The machine parameters for the simulation can be found in [15].

a) Performamnce Result of SG with PM on no-load Condition

In Fig 9 to 11, the voltage buildup of the three-phase generator is illustrated. The profile for phase A is shown in Fig 9. The profile for phase B and C are shown in Fig 10 and 11 respectively. The excitation capacitor value of 80 µF was applied in this arrangement with PM excitation flux value of 0.8 Wb. The results show the generator phase voltage to be above 220 volts. The voltage level is commendable since the generation is operating on no load condition. This is because, when load is added, the generator voltage is expected to drop. Fig. 12 shows the generator power output, which is 1600 W. The power output also shows a smooth and a more stable condition.

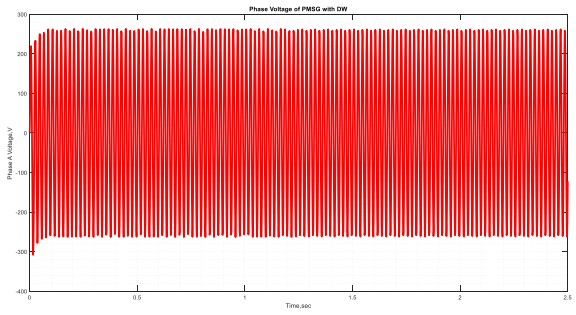

Fig. 9: Phase A voltage the generator on no load condition

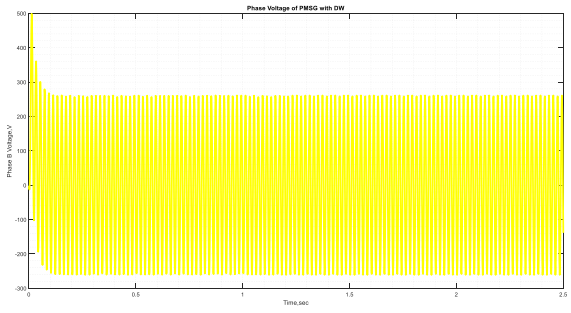

Fig. 10: Phase B voltage the generator on no load condition

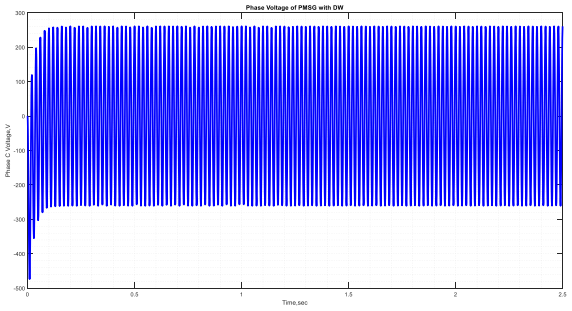

Fig. 11: Phase C voltage the generator on no load condition

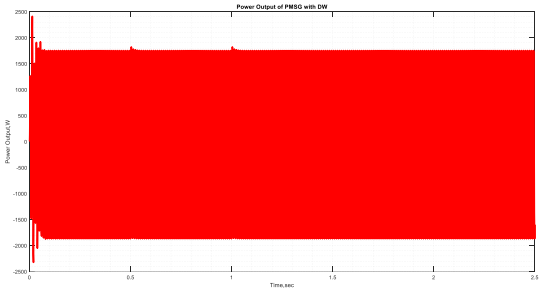

Fig.12 Power output of the generator on no load condition

b) Performamnce Result of SG with PM on sudden addition and removal of load Condition

The effect of varying loading conditions for the generator on voltage, power output, excitation capacitor current, active, and reactive power, and load voltage at constant power factor of value of 0.8 and excitation capacitor of 80 uF is shown in Fig 13 to Fig.19.The generator was first started on no load. It runs till 0.5 sec; then suddenly a load of 400 Ω was applied at 0.8 power factor. The generator initially experienced a hike in voltage when there was no load added. Then, there was voltage downfall on addition of load. This lasted to 2 sec when the load was removed. A climb in the power output was also seen to be about 1800 W when there was no load. The power output drops to 1400 W after the load was added. This is shown in Fig.16. Under the same excitation conditions, it was found that the capacitor current, active, and reactive, as well as the load voltage were very sensitive to the variation in the load values. The measured no-load phase-current of the capacitor of the generator, the active and reactive power and the load voltage is illustrated in Fig 17 to Fig. 19.

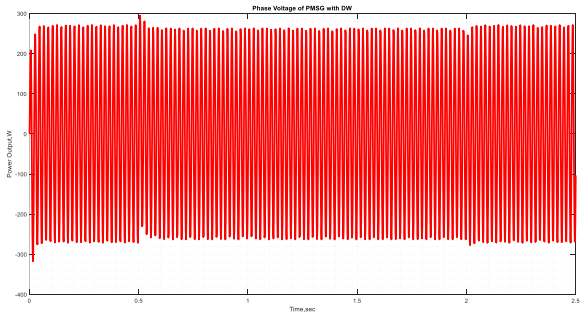

Fig.13 Phase A voltage the generator on load disturbance

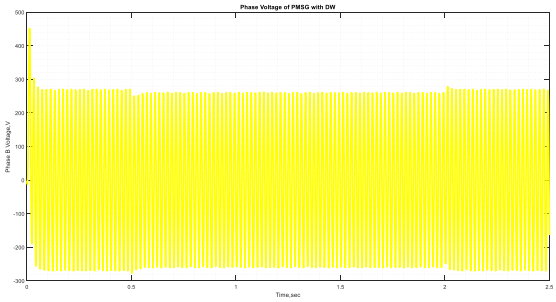

Fig.14 Phase B voltage the generator on load disturbance

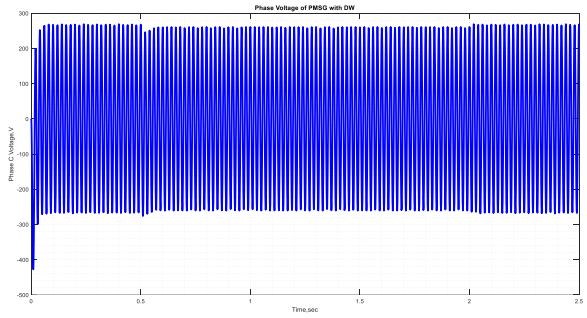

Fig. 15 Phase C voltage the generator on load disturbance

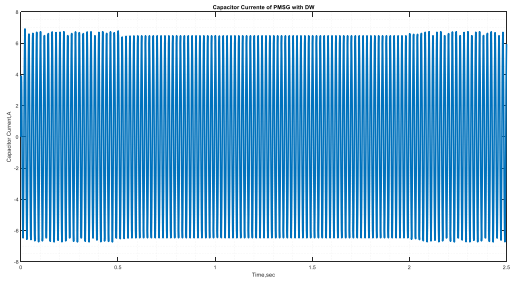

Fig.16 Capacitor current of the generator on load disturbance

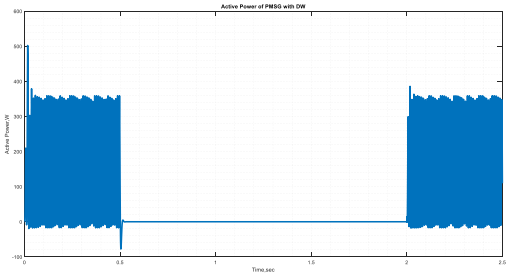

Fig.17 Active power of the generator on load disturbance

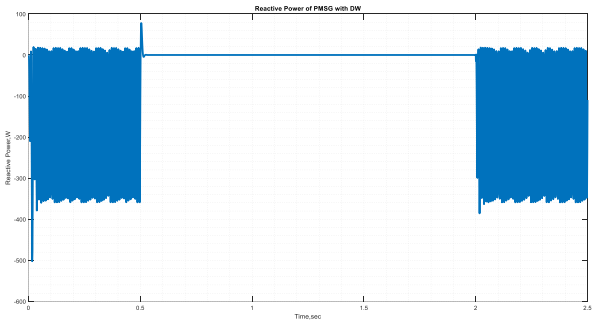

Fig.18 Reactive power of the generator on load disturbance

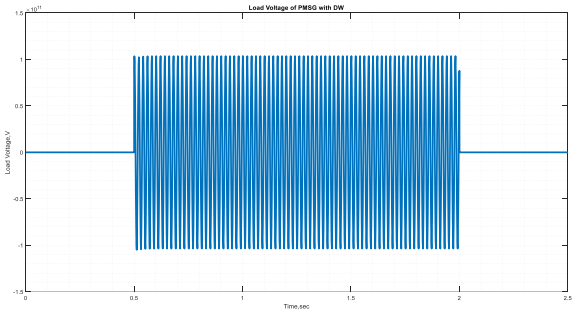

Fig.19 Load voltage of the generator on load disturbance

CONCLUSION

This study has carried out dynamic performance analysis of a self-excited three-phase cageless rotor reluctance generator with permanent magnet based on winding function theory using the actual geometry of the machine for calculation of inductance and analysis of the machine instead of the use of traditional winding function, which uses Fourier model. The calculation also involves the harmonic content of the machine, where all the harmonics are considered including the fundamental components of winding functions. The expression of the machine inductance developed based on winding function theory was used to carry out the dynamic simulation of the machine in natural variable frame. Effect of load variation was studied, and the machine performance changes as the load is varied. The simulation was made using MATLAB/SIMULINK.

REFERENCES

[1] D. Timmons, J. M. Harris, and B. Roach, *The Economics of Renewable Energy*. Global Development and Environment Institute, Tufts University, 2014.

[2] T. R. Ayodele and A. S. O. Ogunjuyigbe, “Wind energy resource, wind energy conversion system modelling and integration: a survey,” *International Journal of Sustainable Energy*, vol. 34, pp. 657–671, 2015.

[3] E. C. Obuah and I. Briggs, “Dynamic characteristic of permanent magnet assisted synchronous reluctance generator,” *International Journal of Electrical Machines & Drives*, vol. 4, no. 1, pp. 1–5, 2020.

[4] A. S. O. Ogunjuyigbe, T. R. Ayodele, and B. B. Adetrkon, "Steady state analysis of wind driven self-excited reluctance generator for isolated application," *Electric Power Systems Research*, vol. 114, pp. 983–1004, 2017.

[5] S. C. Kuo and L. Wang, "Analysis of isolated self-excited induction generator," *IEEE Proceedings on Generation, Transmission and Distribution*, vol. 149, pp. 90–97, 2002.

[6] M. M. Ali, S. M. Allam, and T. H. Abdel-Mondel, "Dynamic characteristics of an isolated self-excited synchronous reluctance generator driven by a wind turbine," *Turkish Journal of Electrical Engineering & Computer Sciences*, vol. 24, pp. 5238–5250, 2016.

[7] A. I. Alolah, "Capacitance requirements for three-phase self-excited reluctance generator," *IEEE Proceedings on Generation, Transmission and Distribution*, vol. 138, pp. 193–198, 1991.

[8] Y. H. A. Rahim, A. L. Mohamadien, and A. S. Al Khalaf, "Comparison between the steady-state performance of self-excited reluctance and induction generators," *IEEE Transactions on Energy Conversion*, vol. 5, no. 3, pp. 519–525, Sep. 1990.

[9] R. M. Reza, "Synchronous reluctance machine (SynRM) in variable speed drives (VSD) applications," Ph.D. dissertation, Royal Institute of Technology, Stockholm, Sweden, 2011.

[10] E. S. Obe and L. U. Anih, "Influence of rotor cage on the performance of a synchronous reluctance generator," *Electric Power Components and Systems*, vol. 38, pp. 960–973, 2010.

[11] E. C. Obuah, O. E. Ojuka, E. I. Wodi, and W. Ikonwa, "Dynamic modelling of a rotor cage permanent magnet synchronous generator with capacitive assistance," *Global Scientific Journals (GSJ)*, vol. 10, no. 6, pp. 211–266, 2022.

[12] D. Staton, T. J. E. Miller, and S. E. Wood, "Maximizing the saliency ratio of the synchronous reluctance motor," *IEE Proceedings B - Electric Power Applications*, vol. 140, no. 4, pp. 249–259, Jul. 1993.

[13] L. Wang and Y. S. Wang, "Dynamic performance and minimum loading effects of an isolated self-excited reluctance generator," *IEEE Power Engineering Society Winter Meeting*, vol. 1, pp. 13–18, 1999.

[14] E. S. Obe and I. K. Onwuka, "Modeling and performance of a self-excited two-phase reluctance generator," *Nigerian Journal of Technology (NIJOTECH)*, vol. 30, no. 2, pp. 58–65, Jun. 2011.

[15] M. Aliyu, "Modelling of permanent magnet synchronous machines in the natural abc frame," Ph.D. dissertation, Dept. of Electrical Engineering, Ahmadu Bello University, Zaria, Nigeria, 2014.